Title: Geophysical model of the hydrothermal system of the Amado Nervo Volcano (Nayarit, Mexico) and preliminary evaluation of its geothermal potential.

Authors: Jimena Itzel Castellanos–Villalpando [a], Mario Alberto Fuentes–Arreazola [b,c*], Ana Mercedes Cupul–Velázquez [b], Nancy Vázquez–Hernández [d], Francisco Javier Núñez–Cornú [c].

a. Universidad de Guadalajara, Centro Universitario del Sur, Licenciatura en Geofísica, Ciudad Guzmán, Jalisco, México.

b. Universidad de Guadalajara, Centro Universitario de la Costa, Departamento de Ciencias Exactas, Ixtapa, Puerto Vallarta, Jalisco, México.

c. Universidad de Guadalajara, Cuerpo Académico (CA276) Sismología y Volcanología de Occidente (SisVOc), Ixtapa, Puerto Vallarta, Jalisco, México.

d. Universidad de Guadalajara, Centro Universitario de Tonalá, Licenciatura en Ingeniería en Energía, Tonalá, Jalisco, México.

* Corresponding author: marioafar@gmail.com

Jimena Itzel Castellanos–Villalpando, https://orcid.org/0009-0006-5400-0286

Mario Alberto Fuentes–Arreazola: https://orcid.org/0000-0002-0568-7302

Ana Mercedes Cupul–Velázquez: https://orcid.org/0009-0007-5406-2679

Nancy Vázquez–Hernández: https://orcid.org/0009-0003-1713-0709

Francisco Javier Núñez–Cornú: https://orcid.org/0000-0003-1515-1349

Abstract

This study presents a conceptual model of the hydrothermal system associated with the Amado Nervo Volcano in western Mexico, integrating geological, gravity, magnetic, and geothermal data. The objectives were to characterize the subsurface structure of the volcanic system, identify geophysical signatures potentially associated with hydrothermal alteration, and provide a preliminary estimate of the region’s exploitable geothermal potential. Aeromagnetic data were processed using reduction to the pole, analytical signal, and upward continuation, and spectral analysis techniques, whereas gravity data were derived from the Global Gravity Model (GGM+) and transformed into simple and residual Bouguer anomalies. The radially averaged power spectrum method was applied to estimate magnetic source depths, the Curie point depth, the geothermal gradient, and conductive heat flow. The geophysical results reveal a special association among magnetic attenuation zones, analytical signal minima, and negative gravity anomalies, delineating structurally complex domains characterized by reduced density and magnetization. Spectral analysis yielded a Curie point depth of approximately 7.5 km, from which a geothermal gradient of 70.8 $^{\circ}C \cdot km^{-1}$ and a conductive heat flow of 176 $mW \cdot m^{-2}$ were estimated. These values are consistent with those reported for geothermal regions of the Trans–Mexican Volcanic Belt. Integration of geophysical and geological information enabled the development of a conceptual hydrothermal model of a structurally controlled volcanic–hydrothermal system potentially sustained by a residual intrusive heat source. A preliminary geothermal resource assessment was conducted using the volumetric Heat in Place method coupled with 9,999 Monte Carlo simulations. The results yielded a mean geothermal potential of 19.75 MW, with simulated values ranging from approximately 5 to 34 MW. Although subject to uncertainties in reservoir geometry and thermophysical parameters, the estimated resource ranks the Amado Nervo volcanic system among medium–scale geothermal prospects in Mexico. The proposed hydrothermal architecture shows similarities to that of the nearby San Pedro Domes geothermal field and supports continued exploration through detailed geophysical, geochemical, and drilling investigations. Overall, this study demonstrates the value of integrating indirect geophysical methods for early–stage geothermal assessment in volcanic regions of the Trans–Mexican Volcanic Belt.

Keywords

Geothermal exploration, Hydrothermal system, Trans–Mexican Volcanic Belt, Potential geophysical data, Amado Nervo Volcano

Highlights

- Integrated magnetic, gravity, and thermal data were used to develop a conceptual hydrothermal model for the Amado Nervo Volcano.
- Spectral analysis of aeromagnetic data allowed estimation of geothermal gradients and conductive heat flow.
- Monte Carlo simulations indicate a medium-scale geothermal potential (≈20 MW), supporting the viability of advanced exploration.

Resumen

Este estudio presenta un modelo conceptual del sistema hidrotermal asociado al Volcán Amado Nervo, en el occidente de México, mediante la integración de información geológica, gravimétrica, magnética y geotérmica. Los objetivos fueron caracterizar la estructura subsuperficial del sistema volcánico, identificar firmas geofísicas potencialmente asociadas a la alteración hidrotermal y proporcionar una estimación preliminar del potencial geotérmico explotable de la región. Los datos aeromagnéticos fueron procesados mediante técnicas de reducción al polo, señal analítica, continuación ascendente y análisis espectral, mientras que los datos gravimétricos se derivaron del Modelo Gravimétrico Global (GGM+) y se transformaron en anomalías de Bouguer simple y residual. El método del espectro de potencia promediado radialmente se aplicó para estimar la profundidad de las fuentes magnéticas, la profundidad del punto de Curie, el gradiente geotérmico y el flujo de calor conductivo. Los resultados geofísicos revelan una asociación entre zonas de atenuación magnética, mínimos de señal analítica y anomalías gravimétricas negativas, delimitando dominios estructuralmente complejos caracterizados por una reducción de la densidad y la magnetización. El análisis espectral permitió estimar una profundidad del punto de Curie de aproximadamente 7.5 km, a partir de la cual se calcularon un gradiente geotérmico de 70.8 $°C \cdot km^{-1}$ y un flujo de calor conductivo de 176 $mW \cdot m^{-2}$. Estos valores son consistentes con los reportados para regiones geotérmicas del Cinturón Volcánico Trans–Mexicano. La integración de la información geofísica y geológica permitió desarrollar un modelo conceptual hidrotermal correspondiente a un sistema volcánico–hidrotermal estructuralmente controlado y potencialmente sustentado por una fuente de calor intrusiva residual. La evaluación preliminar del recurso geotérmico se realizó mediante el método volumétrico Heat in Place acoplado con 9,999 simulaciones de Monte Carlo. Los resultados arrojaron un potencial geotérmico promedio de 19.75 MW, con valores simulados que oscilan entre 5 y 34 MW. Aunque esta estimación está sujeta a incertidumbres relacionadas con la geometría del reservorio y los parámetros termofísicos empleados, el recurso estimado sitúa al sistema volcánico Amado Nervo dentro del rango de prospectos geotérmicos de escala media en México. La arquitectura hidrotermal propuesta presenta similitudes con la del campo geotérmico cercano de Domos de San Pedro y respalda la continuidad de las actividades de exploración mediante investigaciones geofísicas, geoquímicas y de perforación más detalladas. En conjunto, este estudio demuestra el valor de integrar métodos geofísicos indirectos para la evaluación geotérmica en etapas tempranas dentro de regiones volcánicas del Cinturón Volcánico Trans–Mexicano.

Palabras clave

Exploración geotérmica, Sistema hidrotermal, Cinturón Volcánico Trans–Mexicano, Datos geofísicos potenciales, Volcán Amado Nervo

1. Introduction

The Trans–Mexican Volcanic Belt (TMVB) is one of the regions with the highest geothermal potential in Mexico, owing to tectonic activity driven by the subduction of the Rivera and Cocos Plates beneath the North American Plate (Figure 1). This geodynamic configuration favors the development of hydrothermal systems dominated by fluid convection, in which the primary heat source originates from shallow magmatic bodies (Prol–Ledezma and Morán–Zenteno, 2019). Consequently, the TMVB hosts multiple geothermal exploration projects, several of which are currently under commercial operation.

Within this volcanic province, the state of Nayarit contains several volcanic edifices of geothermal significance, including Sangangüey, Ceboruco, San Juan, Tepetiltic, Las Navajas, the San Pedro Domes, and the Amado Nervo Volcano. A key structural feature in the region is the San Pedro–Ceboruco Graben (SPCG), an east–west–trending tectonic depression formed by normal faulting associated with crustal extension in the TMVB. The graben exhibits evidence of recent tectonic activity and Holocene volcanism, conditions that are favorable for the development of active hydrothermal systems (Ferrari et al., 2003). Its central sector hosts the San Pedro Domes geothermal field, with an installed capacity of 35.5 MW, recognized as the first geothermal power plant operated by a private company in Mexico (Reyes–Orozco et al., 2019).

Scientific research in the SPCG has been extensive yet heterogeneous. Several decades ago, the Comisión Federal de Electricidad conducted geological, geophysical, and geochemical surveys, the results of which remain in confidential internal reports. Over the past 30 years, numerous studies have contributed to understanding the region's geology, stratigraphy, and eruptive history (Ferrari et al., 1999, 2003; Petrone et al., 2001; Sieron and Siebe, 2008). Concurrently, a wide range of geophysical investigations, including gravity, magnetic, seismic, and electromagnetic studies, have provided insights into the subsurface structure of the graben (Venegas, 1995; Sánchez et al., 2009; Rodríguez–Uribe et al., 2013; Fernández–Córdoba et al., 2017; Sawires and Aboud, 2019; Núñez–Cornú et al., 2020; Fuentes–Arreazola et al., 2021; Muñoz–Burbano et al., 2024). Additionally, several studies have proposed models of the hydrothermal system hosted within the graben, primarily based on geological information and well data (Reyes–Orozco et al., 2019; Rodríguez et al., 2019).

At the southeastern end of the SPCG lies the Amado Nervo Volcano, a shield–type edifice composed mainly of basaltic lava flows, located in a structural context similar to that of the San Pedro Domes geothermal field. Despite these favorable conditions, this volcano has received comparatively little scientific attention, with most studies focusing on general geological descriptions (e.g., Ferrari et al., 2003). The absence of integrated geophysical studies represents a significant gap in understanding its internal structure and geothermal potential.

To address this gap, the present study integrates aeromagnetic and gravity data with existing geological and hydrogeological information to characterize the geophysical configuration of the Amado Nervo Volcano. Through the analysis and interpretation of potential–field anomalies, we identify key subsurface properties, delineate zones potentially associated with hydrothermal alteration, and propose a preliminary conceptual model and geothermal potential of the hydrothermal system that may be hosted beneath the volcanic edifice. This work represents the first detailed geophysical characterization of the area and provides a robust foundation for subsequent stages of advanced geothermal exploration.

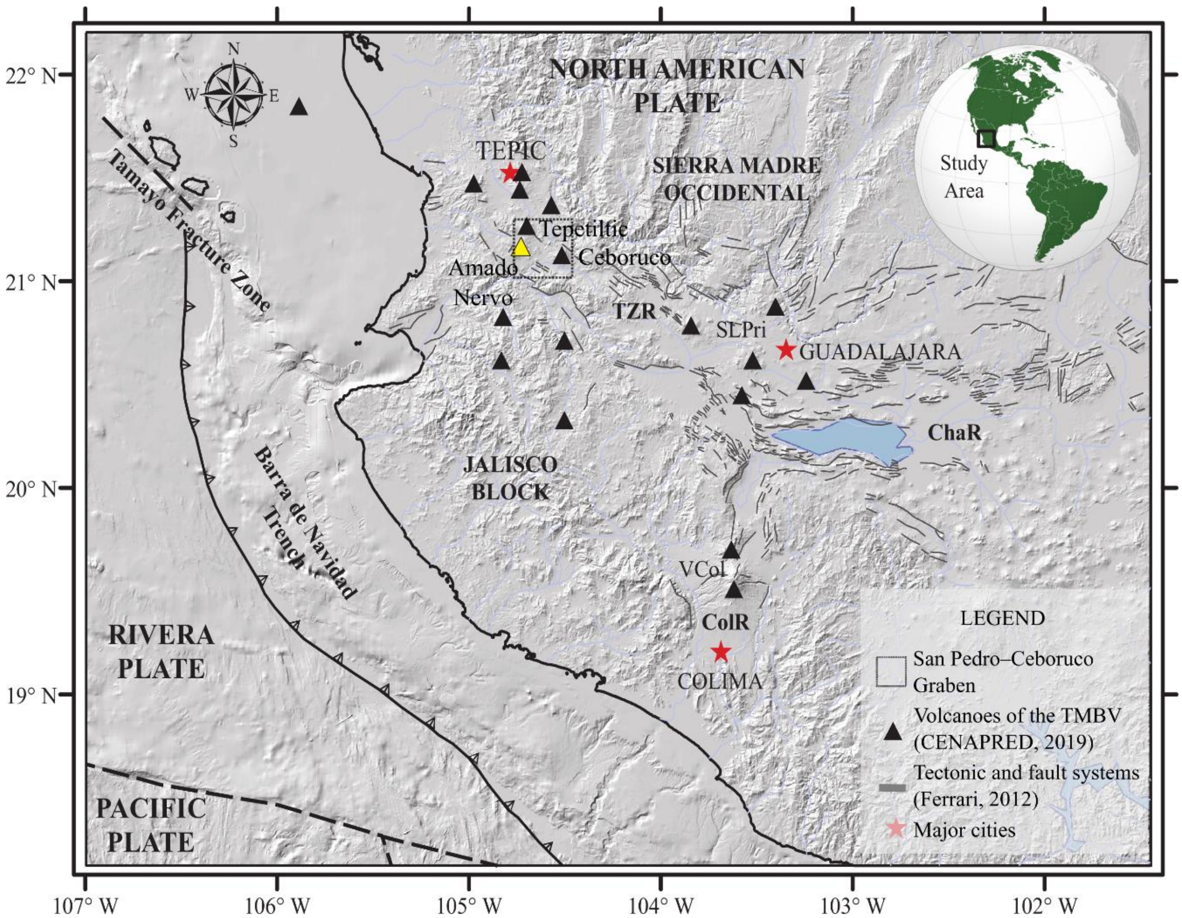

Figure 1. Location map of the Amado Nervo Volcano illustrating its spatial relationship with major tectonic domains and plate boundaries. The Tepic–Zacoalco (TZR), Chapala (ChaR), and Colima (ColR) rift zones are also indicated. Inset: Location of the study area within the American continent. Modified from Fuentes–Arreazola et al. (2021).

2. Study area

2.1. Tectonic–geological setting and eruptive history

The Amado Nervo Volcano is a Quaternary shield volcano (0.22 Ma) located in the state of Nayarit (21.150399°N, –104.756680°W; 1447 m.a.s.l.), near the northwestern limit of the TMVB. It lies within the SPCG, a tectonic structure associated with the Tepic–Zacoalco Rift, which marks the boundary between the Jalisco Block and the North American Plate (Figure 1). Together with the Chapala and Colima rifts, the Tepic–Zacoalco Rift defines a triple–junction zone near the city of Guadalajara (Nelson, 1980; Stock, 1993; Ferrari et al., 2003). This tectonic framework is characterized by crustal extension, normal faulting, and recent volcanism.

The geological evolution of the SPCG spans from the late Miocene to historical times and is marked by shifts in magma composition and tectonic activity (Figure 2). Intense rhyolitic volcanism dominated the early Pliocene (5–4.2 Ma), followed by mafic eruptions associated with regional extension. Around 1.1 Ma, activity evolved into a more differentiated bimodal regime, leading to the formation of the San Pedro–Cerro Grande volcanic complex, including dacitic–andesitic domes and the Tepetiltic stratovolcano (~480 ka) (Ferrari et al., 1999, 2003; Petrone et al., 2001).

A major event in this sequence was the collapse of the San Pedro caldera between ~450 and 283 ka, followed by intracaldera dome growth (e.g., Los Ixletes, Los Ocotes, Cerro Lobos) and the Cuastecomate Plinian eruption (~210 ± 260 ka), which produced widespread pyroclastic deposits. Subsequently, the Amado Nervo Volcano developed (220 ± 29 ka) through the effusion of mildly alkaline basaltic lavas, representing a late effusive stage that contrasts with the predominantly silicic activity of the San Pedro complex (41 ± 20 ka) and suggests magmatic rejuvenation during the Quaternary. The southeastern sector hosts the Ceboruco Volcano, the youngest and most active center (45–0 ka), with historical eruptions [A.D. 930, 1870–1875] (Núñez et al., 2022) and persistent fumarolic activity indicating an active hydrothermal system (Ferrari et al., 2003; Sieron and Siebe, 2008; Núñez–Cornú et al., 2020).

At a more local scale, the Amado Nervo Volcano is situated within the San Pedro–Amado Nervo subgraben, limited by NW–SE and NE–SW–oriented normal faults and by minor strike–slip faults in its southeastern portion (Figure 2). Major structures in this area include the Borbollón, Milpillas–Cerro Grande, and Las Cebollas faults, as well as the Amado Nervo strike–slip fault. This structural configuration strongly influences regional morphology (Reyes–Orozco et al., 2019) and, speculatively, also the fluid circulation.

According to the geological map (Figure 2), constructed using data from INEGI (2023) and the Mexican Geological Survey (SGM, 2023), the study area comprises the following surface lithologies: rhyolitic ignimbrite, pumice–fall deposits, alluvium, Tertiary rhyolitic breccia, Quaternary basaltic lava flow, and Quaternary andesitic lava flow. Locally, sandstone–limestone units may also crop out, although they are more commonly present at depths greater than 400 m. At deeper stratigraphic levels, rhyolitic ignimbrites, calcarenite, Tertiary andesitic lava flows, and granitic bodies are identified. Basaltic breccia is exposed at the eruptive vent of the Amado Nervo Volcano, consistent with its effusive origin.

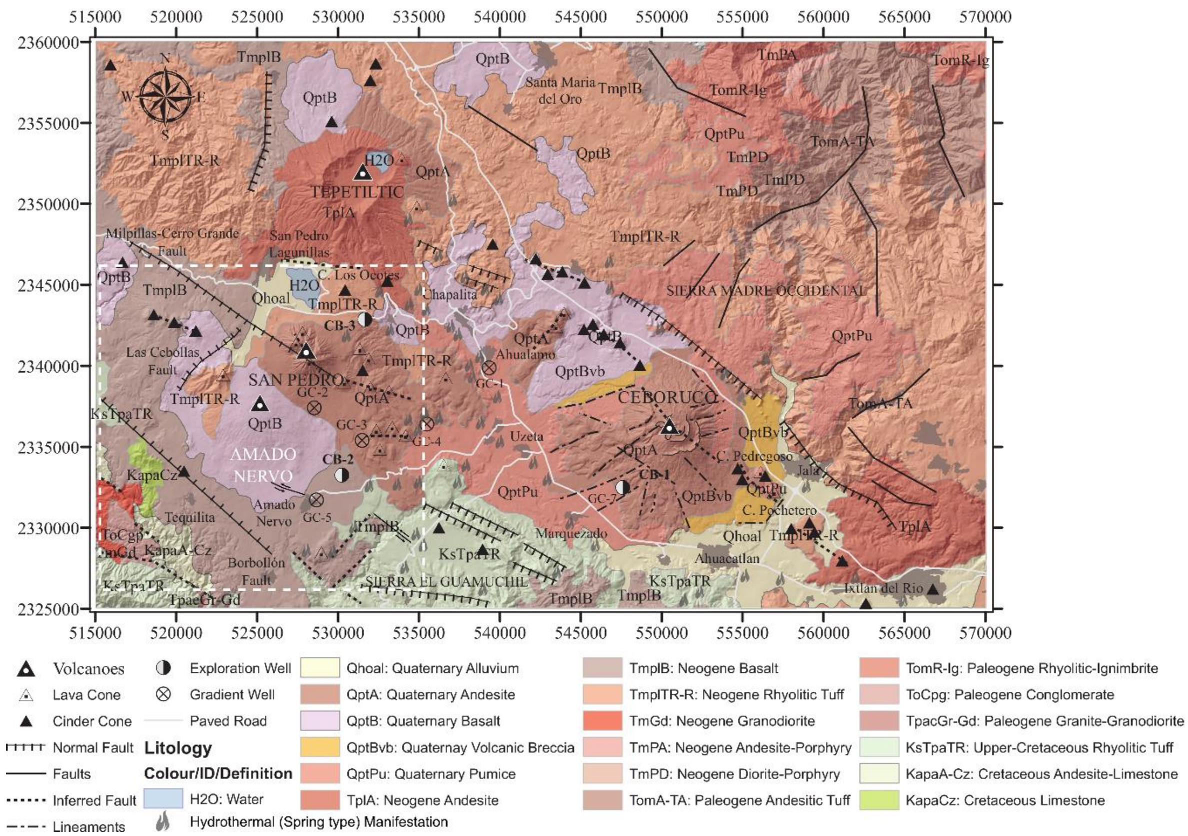

Figure 2. Regional to local geological map of the San Pedro–Ceboruco Graben. Exploration and gradient wells, as well as lava and scoria cones, are shown following Ferrari et al. (2003). Fault traces and lithological units are compiled from Ferrari et al. (2012), SGM (2025), and INEGI (2025). Hydrothermal manifestations location from Tello–Hinojosa (1994). Inset: The dotted white line delineates the specific area analyzed using geophysical data near the San Pedro–Amado Nervo subgraben.

2.2. Hydrogeological and hydrothermal setting

From a hydrological perspective, the region exhibits a predominantly dendritic drainage pattern, transitioning to a radial configuration over the volcanic edifices. Surface runoff and stream channels generally flow toward the southwest. The volcanic units exposed in the study area may exhibit variable porosity and permeability depending on their lithology, degree of fracturing, and volcanic textures. Although quantitative hydrogeological data are currently unavailable for these units, highly fractured zones associated with regional and local structures may plausibly act as preferential pathways for infiltration, groundwater recharge, and fluid circulation within shallow aquifers and potential hydrothermal systems.

Three unconfined aquifers have been identified in the vicinity of Amado Nervo Volcano: Valle de Compostela, Valle de Banderas, and Ixtlán–Ahuacatlán. Although detailed hydrogeological properties of these systems remain poorly constrained, groundwater occurrence and flow are likely influenced by lithological heterogeneity and rock fracturing. Available piezometric information is limited and should be regarded only as a regional hydrogeological reference. For example, groundwater-level measurements obtained during a well-leveling survey conducted in October 2017 indicate that the water table in alluvial deposits near the community of Juan Escutia, approximately 10 km west of the volcano, ranged between 10 and 30 m below ground surface (CONAGUA, 2025). The referenced report also indicates that slight groundwater-level declines typically begin in November due to agricultural groundwater extraction following the rainy season. Because these measurements correspond to a nearby alluvial aquifer rather than the volcanic edifice itself, they are presented solely to provide a general regional context regarding groundwater occurrence and flow conditions.

The geochemical study of hot springs surrounding the Ceboruco Volcano (Figure 2), conducted by Tello–Hinojosa (1994), revealed an active hydrothermal system linked to both the volcanic edifice and its immediate structural framework. The hydrothermal manifestations exhibit chemical compositions consistent with the heating of meteoric waters that infiltrate through highly permeable zones, primarily fractures and faults associated with the regional geological–structural configuration. These fluids then recirculate toward the surface, driven by elevated thermal gradients.

Within this regional setting, geothermal gradient measurements from nearby exploratory wells indicate significant thermal anomalies around the Amado Nervo Volcano (Figure 2): GC–5 (~6.9 km south–southeast) with 53.2 °C·km^{-1}; CB–2 (~6.1 km southeast) with 102.5 °C·km^{-1}; GC–3 (~7 km east–southeast) with 103.6 °C·km^{-1}, and CB–3 (~7.8 km northeast) with 52.4 °C·km^{-1} (Espinoza–Ojeda et al., 2023). These values support the presence of a high–temperature regime consistent with the development of deep hydrothermal systems.

Additionally, the geochemical signatures, including characteristic concentrations of silica, bicarbonate, and other major ions, suggest a medium– to high–temperature reservoir influenced by water–rock interaction processes. The spatial distribution of springs and their alignment with major structural lineaments further indicate that hydrothermal flow is channeled along faults that serve as preferential pathways for upward fluid migration.

3. Data and method of analysis

3.1. Geophysical data

The aeromagnetic data used in this study were obtained from a 1983 survey conducted by the Mexican Geological Survey (SGM, 2005). The survey was carried out using GPS navigation along flight lines spaced 1,000 m apart, at an average elevation of 300 m above ground level. The total magnetic field was computed after applying corrections for aircraft motion, diurnal variation, and flight–line leveling. The residual magnetic field (RMF) was derived by subtracting the International Geomagnetic Reference Field (IGRF, 1980), using reference values of total intensity (43,415 nT), inclination (47°49’), and declination (8°52’). The SGM produced a 1:50,000–scale contour map of the RMF with 10 nT contour intervals. For this study, a digital ASCII grid with 200 m spacing and an extent of 20 × 20 km (400 km²) was acquired from the SGM and centered near the Amado Nervo Volcano. This grid served as the basis for aeromagnetic processing and analysis.

In this study, gravity data from the Global Gravity Model GGM+ (Hirt et al., 2013) were used. This model is a modern tool for regional gravity analysis, integrating satellite measurements from missions such as GRACE and GOCE. GGM+ provides an approximate spatial resolution of 200 m, comparable to the station spacing typically employed in terrestrial gravity surveys for local characterization of volcanic structures. Binary files corresponding to the N20W105 cell were downloaded, containing gravity acceleration values (N20W105.ga) and gravity disturbance values (N20W105.dg). From these files, data within the study area were extracted, yielding a grid of 90 rows by 97 columns (8,730 nodes) that served as the basis for regional analysis and geophysical interpretation.

3.2. Aeromagnetic and gravimetric data processing and analysis

The residual magnetic field data were processed through a series of standard transformations, including reduction to the pole (RTP), analytic signal amplitude, and upward continuation, to enhance magnetic source signatures and facilitate geological interpretation. Following the RTP transformation, the workflow described by Fuentes–Arreazola et al. (2023) and references therein was applied to compute and correct the radially averaged power spectrum. This spectral analysis enabled estimation of the upper and lower depths of the magnetic sources responsible for the observed anomalies. The lower bound of these sources was interpreted as the Curie Point Depth, from which the thermal gradient and conductive heat flow were subsequently estimated following the formulations of Turcotte and Schubert (2002).

The gravity disturbance data derived from the GGM+ model correspond to Free–Air Anomaly values, defined as the difference between the measured gravity at a specific point on Earth's surface and the theoretical gravity, after correction for elevation and the atmospheric mass between the terrain surface and the satellite (Seigel, 1995; Hildenbrand et al., 2002). From these disturbance values, the observed gravity at each hypothetical station was reconstructed. Latitude, elevation, and Bouguer slab corrections were then applied to compute the simple Bouguer anomaly (Telford et al., 1990; Seigel, 1995). To isolate the local residual gravity field, a band–pass filter with a long–wavelength cutoff of 20 km, corresponding to the lateral extent of the analyzed grid, was applied to remove regional trends.

From the RTP magnetic anomaly upward continued to 1 km, together with the residual simple Bouguer anomaly, a 10–km–extended west–east profile was extracted across the study area. This profile was subsequently modeled to approximate the regional geological framework. All aeromagnetic and gravimetric processing steps, including data reduction, spectral analysis, filtering, and potential–field transformations, were carried out using Oasis montaj software (Seequent Ltd., Christchurch, New Zealand).

3.3. Geothermal potential assessment

The volumetric Heat in Place method is commonly used in preliminary geothermal assessments to estimate the thermal energy stored within a volume of hot rock. The recoverable thermal energy [Q_{rec}] can be expressed as (Equation 1):

$$Q_{rec} = R_g V[\phi \rho_w c_w + (1 - \phi)\rho_r c_r](T_r - T_{ref}) \quad \text{Eq.1}$$

where, V is the reservoir volume, ϕ is the porosity, ρ is the water and rock densities, c is the water and rock specific heat, T_r is the reservoir temperature, T_{ref} is the reference temperature, and R_g is the recovery factor.

To account for parameter uncertainty, Monte Carlo simulations were performed using a custom MATLAB script developed for this study following the methodology described by Muffler and Cataldi (1978), Hiriart–Le Bert et al. (2011), and Garg and Combs (2015). The simulations generated probabilistic estimates of geothermal potential, and the distribution's mean was adopted as the most likely resource estimate.

4. Results

4.1. Gravimetric and magnetic anomalies

The geophysical results are presented beginning with the gravimetric anomalies, followed by the magnetic anomalies and their transformations. Together, these observations provide the basis for developing the hydrothermal conceptual model and for assessing the geothermal potential of the study area.

The simple Bouguer anomaly ranges from –81.74 mGal to –149.13 mGal and exhibits a well–defined regional trend across the study area (Figure 3a). Higher values (~–90 mGal) occur in the southwestern sector, whereas lower values (~–120 mGal) are concentrated toward the northeast. Subtle gravity gradients are observed throughout the area, several of which are spatially coincident with major northwest–southeast structural features, including the Borbollón and Milpillas–Cerro Grande faults.

At the local scale, the Amado Nervo Volcano (ANV) is located within a domain characterized by intermediate Bouguer anomaly values of approximately –116 mGal, whereas Cerro Las Tetillas coincides with a relative gravity minimum of approximately –129 mGal. The San Pedro Domes are situated within a well–defined circular anomaly that reaches minimum values of approximately –140 mGal. The geothermal wells of the San Pedro Domes project are located in the northeastern sector of this anomaly, within an area characterized by negative Bouguer anomaly values relative to the surrounding region.

To isolate the local gravity response, a band–pass filter with a long–wavelength cutoff of 20 km, corresponding to the lateral extent of the data block, was applied. The resulting residual Bouguer anomaly (Figure 3b) ranges from –29.62 mGal to 15.53 mGal, with a mean value of 0.02 mGal. After removing the regional trend, a continuous negative anomaly is observed beneath both the Amado Nervo Volcano and Cerro Las Tetillas. The residual anomaly reaches –4.32 mGal at the ANV and attains its lowest value at Cerro Las Tetillas (–17.83 mGal). This negative domain is located between the Las Cebollas fault to the northwest and the Milpillas–Cerro Grande fault to the northeast.

Higher residual values are observed south, east, and northeast of the Amado Nervo Volcano. In contrast, the San Pedro Domes coincide with a well–defined negative residual anomaly, with values below –20 mGal.

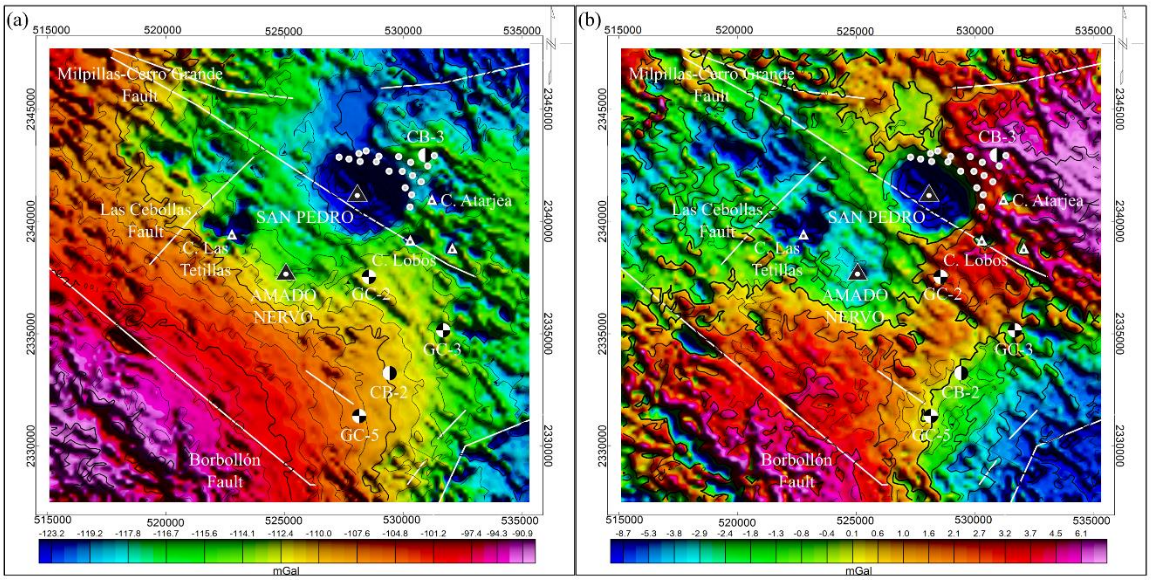

Figure 3. (a) Simple Bouguer and (b) residual/local Bouguer anomaly map of the Amado Nervo Volcano and surrounding areas. Colors and contour lines represent the distribution of gravity anomaly intensities. White lines correspond to geological faults compiled from INEGI (2025) and SGM (2025). Triangular symbols indicate volcanic structures (Ferrari et al., 2003). Circles with alternating fill mark the locations of geothermal exploration wells (CB–2 and CB–3) and gradient wells (GC–2, GC–3, and GC–5) reported by Ferrari et al. (2003). Solid white–gray circles denote the wells of the Domos de San Pedro geothermal project.

Figure 4a displays the residual magnetic field anomaly of the Amado Nervo Volcano and surrounding areas, with values ranging from –337.20 to 1,120.86 nT. Positive anomalies occur primarily over the central sector and toward the south, coinciding with the Amado Nervo Volcano edifice and the San Pedro Domes. An additional positive domain is observed to the northeast in the vicinity of Tepetiltic Volcano, whereas negative anomalies are distributed along the western, northern, and eastern margins of the Amado Nervo Volcano. A well–defined dipolar anomaly is observed at the volcanic vent, characterized by magnetic values ranging from approximately –157 nT to 630 nT. The boundaries of the principal anomaly are spatially coincident with the Borbollón, Las Cebollas, and Milpillas–Cerro Grande faults systems.

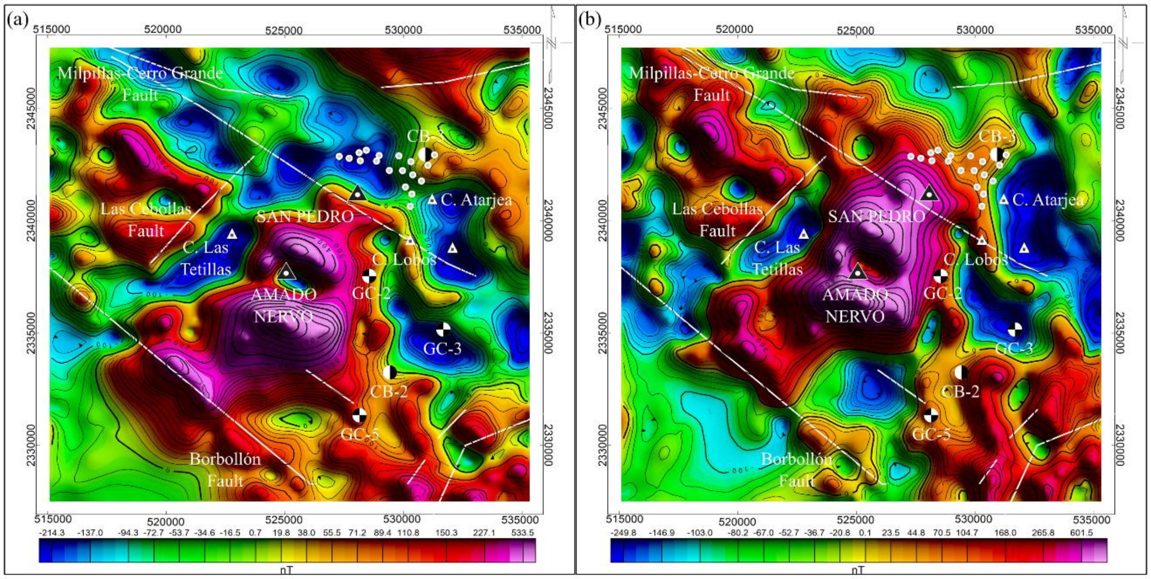

Figure 4. (a) Residual magnetic field and (b) magnetic field reduced to the magnetic pole anomaly map of the Amado Nervo Volcano and surrounding areas. Colors and contour lines represent the distribution of magnetic field intensities.

To remove the effects of magnetic field declination and inclination, the total magnetic field data were transformed to the magnetic pole (Figure 4b). The resulting anomaly ranges from –485.46 nT to 1,391.61 nT and exhibits a predominant northwest–southeast orientation. The principal anomaly remains centered on the Amado Nervo Volcano and comprises three high–intensity lobes with amplitudes of 1,384 nT, 1,061 nT, and 976 nT together with a fourth lower–intensity lobe of 135 nT. The anomaly boundaries are spatially coincident with major regional faults.

To better isolate the magnetic sources within the study area, the analytical signal of the reduced–to–the-pole magnetic anomaly was calculated (Figure 5a). The Amado Nervo Volcano exhibits analytical signal values of approximately 1.30 nT·m⁻¹, whereas the San Pedro Domes are characterized by values of approximately 0.50 nT·m⁻¹. Other volcanic structures also exhibit notable analytical signal amplitudes: Cerro Tetillas, located northwest of the Amado Nervo Volcano, exhibits a value of

0.83 nT·m⁻¹, whereas Cerro Lobos, situated southeast of the San Pedro Domes, reaches 1.05 nT·m⁻¹ and is spatially aligned with the Milpillas–Cerro Grande fault. Three of the five geothermal gradient wells are located in zones with low analytical signal values ranging from 0.07 to 0.15 nT·m⁻¹. Similarly, wells from the San Pedro Domes geothermal project occur in areas with analytical signal values between 0.03 and 0.30 nT·m⁻¹.

To obtain a regional perspective of the magnetic field, a 1 km upward continuation was applied to the reduced–to–the–pole anomaly (Figure 5b). The resulting anomaly ranges from –157 to 580 nT. Following continuation, the principal magnetic anomaly remains prominent, with amplitudes approaching 500 nT, and remains spatially associated with the Amado Nervo Volcano.

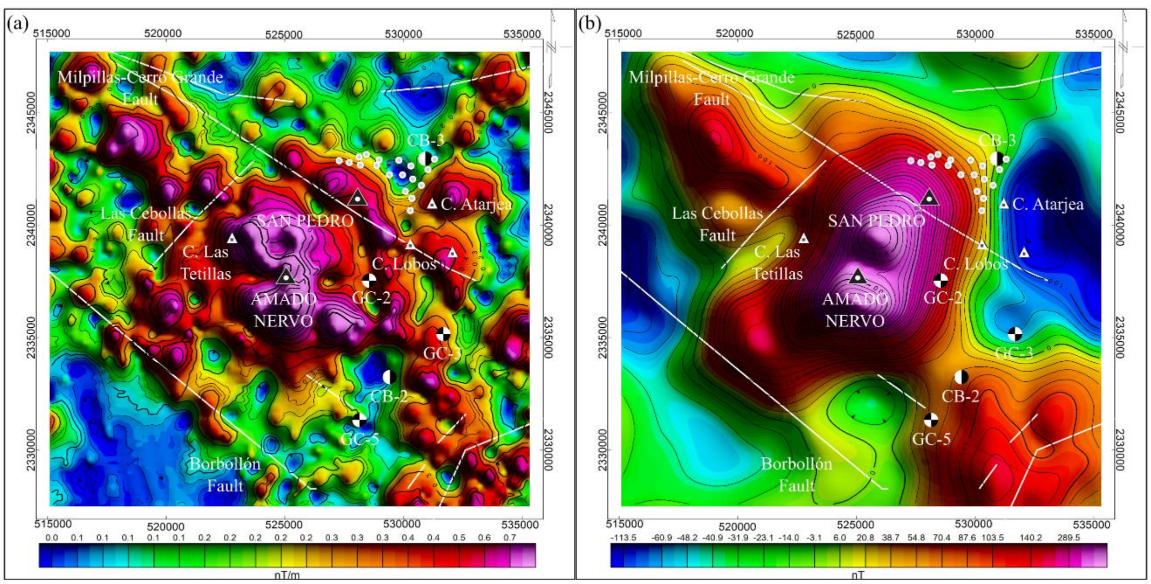

Figure 5. (a) Analytical signal of the residual magnetic field reduced to the magnetic pole, and (b) upward–continued (1 km) anomaly map of the Amado Nervo Volcano and surrounding areas.

4.2. Hydrothermal conceptual model

The hydrothermal conceptual model for the Amado Nervo volcanic system was developed by integrating geophysical, geothermal, and geological information (Figure 6). Spectral analysis of the reduced-to-the-pole magnetic anomaly was used to constrain the depth distribution of magnetic sources and estimate the lower magnetic boundary. Together with gravimetric anomalies, magnetic anomaly patterns, mapped structural features, and available geothermal data, these results provide the framework for the proposed model.

Magnetic source depths were estimated from a radially averaged power spectrum calculated over a 20 × 20 km block of the reduced–to–the–pole anomaly. Using the spectral slope analysis of Ravat et al. (2007) and Fedi et al. (1997), the centroid depth was estimated at Z_0 = –4.34 km and the top of the magnetic sources at Z_t = –1.18 km. Applying the methodology of Okubo et al. (1985) and Tanaka et al. (1999), the lower bound of the magnetic source was estimated at Z_B = –7.50 km.

Assuming Z_B corresponds to the Curie point depth and using a Curie temperature of approximately 580 °C, a geothermal gradient of 70.79 °C·km^{-1} was calculated following Núñez–Demarco et al. (2020), using a surface temperature of 28 °C and a flight altitude of 0.3 km. Using a thermal conductivity of 2.5 W·m^{-1}·°C^{-1} (Turcotte and Schubert, 2002), a conductive heat flow of approximately 176 mW·m^{-2} was obtained. Based on the estimated geothermal gradient, subsurface temperatures were calculated as a function of depth, yielding approximately 150 °C at 1.5–1.7 km depth and exceeding 700 °C at approximately 11 km depth.

The conceptual model comprises a shallow volcanic sequence overlying deeper basement rocks and intrusive units. A transition in geophysical properties is identified near sea level, corresponding to the boundary between volcanic and deeper lithological domains. Geothermal gradient wells, magnetic anomalies, gravity anomalies, and mapped structural features were integrated to define the principal components of the proposed hydrothermal system.

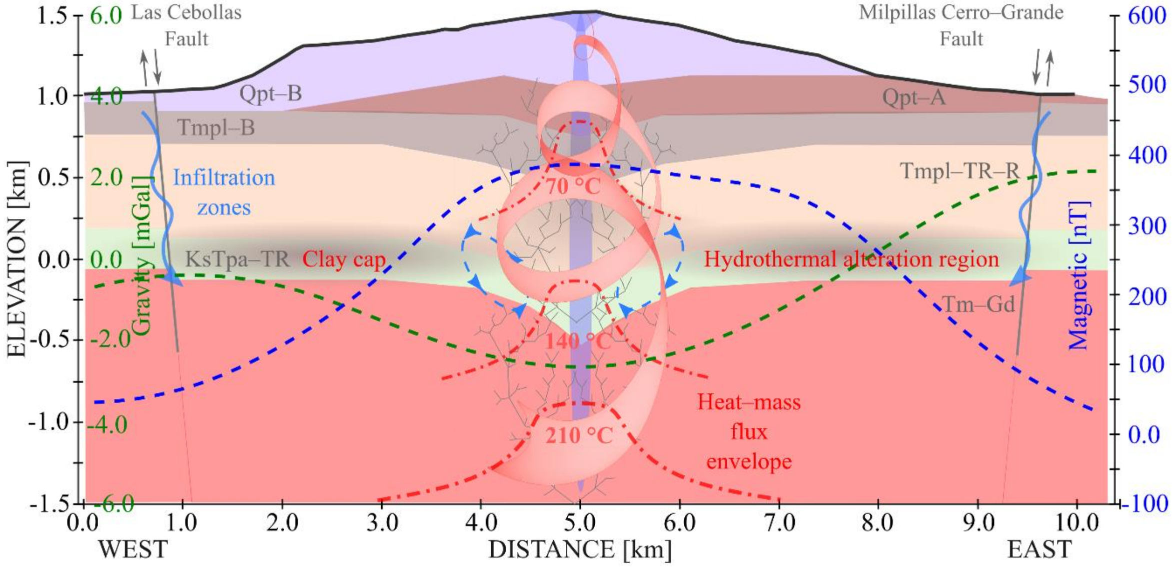

Figure 6. Conceptual hydrothermal model of the Amado Nervo volcanic system. The inset illustrates the residual gravity anomaly and the 1-km upward-continued magnetic anomaly along a 10-km west–east profile. Geological units correspond to those shown in Figure 2. Regional fault systems are incorporated as structural features associated with fluid recharge, permeability enhancement, and hydrothermal fluid migration.

4.3. Geothermal potential estimation

The conceptual model proposes a potential geothermal reservoir located beneath the inferred cap–rock sequence and hosted within fractured crystalline basement rocks intruded by intermediate–composition bodies. The model identifies this domain as a potential target for future exploratory drilling.

The integration of magnetic, gravity, and geothermal–gradient data reveals a spatial association between negative magnetic anomalies, analytical signal attenuation, negative gravity anomalies, and elevated geothermal gradients. These features define geophysical domains characterized by contrasting physical properties within the study area.

The proposed conceptual model exhibits several similarities to the San Pedro Domes geothermal field. In both areas, hydrothermal alteration zones occur at depths of approximately 1 km, temperatures near 150 °C have been reported or estimated, and crystalline basement rocks of the Jalisco Block occur at depths of approximately 1.2–1.8 km beneath volcanic sequences (Reyes–Orozco et al., 2019).

A set of key parameters derived from geological, geophysical, and geothermal data was integrated into a volumetric Heat in Place model coupled with Monte Carlo simulations (Table I). Based on a MATLAB implementation developed for this study and 9,999 simulations, a mean geothermal potential of 19.75 MW with an uncertainty of ±14.41 MW was estimated. The resulting distribution spans approximately 5 MW under conservative scenarios to approximately 34 MW under more favorable conditions.

Table 1. Range of values for the variables involved in the volumetric model used to estimate geothermal potential.

Variables for the Volumetric (Heat In Place) Model		
Parameter	Minimum value	Maximum value
Project lifetime [years]	25	35
Separation pressure [bar]	5	12
Reservoir area [km^2]	1	15
Reservoir thickness [km]	0.10	1.50
Reservoir temperature [°C]	140	250
Ambient temperature [°C]	20	35
Reservoir rock porosity [%]	0.01	0.17
Reservoir rock density [$kg \cdot m^{-3}$]	2400	2900
Reservoir rock specific heat [$kJ \cdot kg^{-3} \cdot °C^{-1}$]	0.60	1.20
Reservoir recovery factor [%]	0.05	0.25
Cycle efficiency [%]	0.10	0.25

5. Discussion

5.1. Geophysical interpretation of gravity and magnetic anomalies

The gravimetric anomalies reveal significant spatial variations that may reflect changes in subsurface density and structural conditions across the Amado Nervo volcanic complex. At the regional scale, the southwest–northeast decrease in Bouguer anomaly values suggests the presence of large–scale density contrasts, while the spatial coincidence between gravity gradients and the Borbollón and Milpillas–Cerro Grande fault systems indicates that regional structures may influence the distribution of these contrasts. Although the observed gradients are subtle, they could be associated with lithological boundaries, zones of enhanced fracturing, or other structurally controlled heterogeneities within the volcanic system.

Local gravity anomalies further highlight variations in the physical properties of the volcanic centers. The intermediate Bouguer anomaly values associated with the Amado Nervo Volcano contrast with the pronounced gravity minima observed at Cerro Las Tetillas and the San Pedro Domes. These negative anomalies may reflect reduced bulk density resulting from enhanced fracturing, hydrothermal alteration, volcanic deposits with elevated porosity, structural collapse, or a combination of these processes. The continuous negative residual anomaly extending beneath both the Amado Nervo Volcano and Cerro Las Tetillas suggests that these volcanic centers may be linked by a common subsurface domain characterized by reduced density. Likewise, the distribution of residual anomalies around the volcanic complex, including relatively high values south, east, and northeast of the Amado Nervo Volcano, points to significant lateral heterogeneity in subsurface properties. These higher residual values may correspond to denser lithological units or structurally coherent blocks that have experienced comparatively limited alteration.

The geometry and spatial distribution of the gravity anomalies further emphasize the importance of tectonic controls. The negative residual anomaly shared by the Amado Nervo Volcano and Cerro Las Tetillas is located between the Las Cebollas and Milpillas–Cerro Grande faults, suggesting that regional fault systems may influence the distribution of density contrasts and the organization of subsurface structures. More broadly, the occurrence of the Amado Nervo Volcano, Cerro Las Tetillas, and the San Pedro Domes within a continuous negative gravimetric domain is consistent with a regionally extensive zone of reduced density and structural complexity. This interpretation agrees with the structural model of Reyes–Orozco et al. (2019), which describes a southeastward–deepening faulted block system beneath the San Pedro Domes area, and with the tectonic framework proposed by Venegas (1995), in which the San Pedro–Tepetiltic Block represents the most subsided structural domain in the region. Such structural depressions may constitute long–lived zones of crustal weakness that favor magma ascent and volcanic activity within the San Pedro–Ceboruco Graben.

Taken together, the gravity data suggest that the Amado Nervo volcanic complex is characterized by pronounced density heterogeneity controlled by both volcanic and tectonic processes. Although the origin of individual anomalies cannot be uniquely determined from gravity data alone, the regional and residual anomaly patterns are consistent with a structurally complex volcanic system shaped by fault–controlled deformation, volcanic construction, and density–reducing processes such as fracturing and alteration.

The magnetic anomalies provide complementary constraints on the structural and magmatic framework of the Amado Nervo volcanic system. At the regional scale, the residual and reduced-to-the-pole magnetic anomaly maps reveal a heterogeneous magnetic fabric characterized by positive magnetic domains associated with the Amado Nervo Volcano, the San Pedro Domes, and other volcanic centers, as well as magnetic lows distributed along the margins of the volcanic complex. The spatial correspondence between several magnetic gradients and major fault systems suggests that tectonic structures may have significantly influenced the distribution of magnetic contrasts and the organization of the volcanic edifice.

The prominent dipolar anomaly centered on the Amado Nervo Volcano suggests the presence of a strongly magnetized source beneath the volcanic edifice. Similar magnetic signatures are commonly associated with basaltic volcanic rocks, shallow intrusive bodies, or volcanic units that preserve significant remanent magnetization (Blakely, 1995; Telford et al., 1990). Furthermore, the reduced-to-the-pole anomaly map reveals a series of northwest–southeast–trending magnetic domains whose boundaries closely coincide with the principal regional faults. The clustering of high–amplitude magnetic lobes beneath the volcano may indicate the presence of multiple magnetized bodies or distinct volcanic units contributing to the overall magnetic response. Together, these observations suggest that tectonic and magmatic processes have jointly influenced the present–day magnetic fabric of the volcanic complex.

The upward continuation results provide additional evidence regarding the scale and continuity of the magnetic sources. The persistence of the principal anomaly following 1 km upward continuation indicates that a substantial component of the magnetic field is associated with sources extending beyond the shallowest levels of the subsurface. This behavior may reflect the presence of a consolidated volcanic conduit, intrusive complexes, or accumulations of mafic volcanic material that retain strong magnetic properties at depth. The continuity of the anomaly from shallow to deeper levels is therefore consistent with a structurally coherent magmatic system beneath the Amado Nervo Volcano.

Magnetic contrasts within the volcanic complex also provide insight into possible alteration–related processes. The subdued magnetic response observed within the central volcanic sector contrasts with the higher–intensity magnetic lobes surrounding the edifice. This pattern may reflect differences in magnetic mineral preservation, whereby hydrothermal alteration and prolonged fluid–rock interaction reduce bulk remanent magnetization in the central sector, while peripheral volcanic units retain a larger proportion of their original magnetic mineral assemblages. Similar magnetic signatures have been documented in other volcanic–hydrothermal systems where alteration is concentrated near eruptive centers and structurally controlled fluid pathways (e.g., Okubo et al., 1985; Fuentes–Arreazola et al., 2023).

The analytical signal results provide additional evidence. The contrast between the relatively high analytical signal amplitudes observed at the Amado Nervo Volcano and the lower values associated with the San Pedro Domes suggests significant differences in the magnetic characteristics of their subsurface sources. The lower amplitudes at the San Pedro Domes may reflect diffuse magnetic boundaries resulting from hydrothermal alteration, structural disruption, or enhanced fracturing. The spatial relationship between analytical signal boundaries and regional fault systems further suggests that tectonic structures may have influenced both the emplacement of magnetic sources and their subsequent modification. Likewise, the analytical signal responses observed at Cerro Las Tetillas and Cerro Lobos indicate that significant magnetic sources occur throughout the volcanic field. At the same time, the alignment of Cerro Lobos with the Milpillas–Cerro Grande fault highlights the potential role of regional structures in controlling volcanic emplacement.

Taken together, the magnetic anomalies, analytical signal patterns, and upward–continuation results support a model in which the interaction between magmatic and tectonic processes controls the Amado Nervo volcanic system. Regional fault systems appear to influence the geometry and distribution of magnetic sources, while alteration–related processes may locally modify magnetic properties. The persistence of major magnetic anomalies at depth, combined with evidence for magnetic attenuation in specific sectors, suggests that the volcanic complex is underlain by a long–lived magmatic framework that continues to influence its structural evolution.

The combined gravity and magnetic signatures support the interpretation of a structurally controlled volcanic framework characterized by pronounced density and magnetic contrasts. Gravity lows, magnetic attenuation, and variations in the analytical signal delineate sectors that have experienced varying degrees of structural disruption and physical–property modification, whereas persistent magnetic highs define the broader magmatic architecture of the volcanic complex. Although the individual geophysical datasets are inherently non–unique, their spatial convergence provides a coherent framework for evaluating the hydrothermal architecture and thermal evolution of the Amado Nervo volcanic system.

5.2. Hydrothermal architecture and thermal constraints

The integrated geophysical interpretation provides the basis for evaluating the thermal structure and hydrothermal architecture of the Amado Nervo volcanic system. In particular, the spectral analysis of magnetic sources offers additional constraints on the depth distribution of thermally significant crustal domains. The estimated lower magnetic boundary (Z_B = 7.50 km) may approximate the Curie point depth, implying that ferromagnetic minerals lose their magnetization at relatively shallow crustal levels. Assuming this interpretation is valid, the derived geothermal gradient (70.79 $^{\circ}C\cdot km^{-1}$) and conductive heat flow (~176 $mW\cdot m^{-2}$) indicate a thermal regime that is elevated relative to typical continental crust and comparable to values reported for geothermal regions within the Trans–Mexican Volcanic Belt (150–200 $mW\cdot m^{-2}$; Prol–Ledezma and Morán–Zenteno, 2019). Furthermore, the close agreement between the spectral geothermal gradient (70.79 $^{\circ}C\cdot km^{-1}$) and the independent borehole–based estimate of 77.92 $^{\circ}C\cdot km^{-1}$ reported by Espinoza-Ojeda et al. (2023) lends support to the reliability of the spectral approach and reinforces the interpretation of a thermally active volcanic–hydrothermal system beneath the Amado Nervo complex.

The depth distribution of magnetic sources suggests a vertically organized volcanic system extending from shallow hydrothermal domains to deeper magmatic levels. The upper magnetic domain, above approximately 1.2 km depth, may have been modified by hydrothermal alteration, oxidation, fracturing, or by volcaniclastic deposits characterized by reduced magnetic susceptibility. In contrast, the deeper magnetic sources may be associated with intrusive rocks of the Jalisco Block described by Reyes-Orozco et al. (2019), providing a plausible explanation for the observed magnetic layering. Although no direct geophysical evidence confirms the existence of an active magma chamber, the persistence of magnetic sources at depth, together with the elevated geothermal gradient, is consistent with the presence of a residual intrusive body that supplies heat to the hydrothermal system. Similar interpretations have been proposed for other volcanic geothermal systems where deep intrusive complexes provide long–lived thermal input despite the absence of active silicic magma reservoirs (Henley and Ellis, 1983; Arnason, 1995).

The conceptual model further suggests that the transition in geophysical properties identified near sea level may correspond to an important lithological boundary separating the volcanic edifice from deeper intrusive and basement rocks. If this interface represents a significant permeability contrast, it could contribute to the development of a cap–rock system that restricts vertical fluid migration and promotes the accumulation of geothermal fluids at depth. Beneath this level, the fractured crystalline basement and associated intrusive bodies may provide the structural framework for geothermal fluid storage and circulation.

Based on the estimated geothermal gradient, temperatures of approximately 150 °C are expected at depths of 1.5–1.7 km (0–200 m.b.s.l.), near the inferred base of the cap–rock sequence. These temperatures fall within a range commonly considered suitable for geothermal development. In the proposed hydrothermal framework, meteoric recharge may occur through fractured volcanic units and fault–controlled permeable zones, allowing groundwater to penetrate toward deeper thermally anomalous sectors. Subsequent mixing between ascending thermal fluids (Heat–mass flux envelope) and cooler meteoric waters may promote cooling and vapor condensation, potentially explaining the absence of fumarolic manifestations and the occurrence of intermediate–temperature springs characteristic of secondary–condensation hydrothermal systems, identified in the vicinity of Amado Nervo Volcano (Tello–Hinojosa, 1994).

Structural controls appear to play a fundamental role in organizing the hydrothermal system. The regional Borbollón, Las Cebollas, and Milpillas–Cerro Grande fault systems define major zones of crustal weakness that likely influenced volcanic emplacement and may continue to govern fluid circulation. The coincidence of gravity lows, magnetic attenuation, and analytical signal minima with sectors affected by faulting suggests that fracturing and structural permeability are concentrated within specific portions of the volcanic complex. In this framework, meteoric recharge may occur through fault–controlled pathways and fractured volcanic units, whereas heat transfer and hydrothermal circulation are focused within structurally favorable sectors of the basement and volcanic succession.

The spatial relationship between geothermal wells and geophysical anomalies provides additional support for this interpretation. Geothermal production wells at San Pedro Domes are located along the margins of the principal gravity low, whereas geothermal–gradient wells are preferentially associated with domains characterized by subdued analytical signal amplitudes and locally elevated geothermal gradients. Although the specific causes of these geophysical signatures are not unique, their recurrent association with geothermal manifestations suggests that density reduction, magnetic attenuation, and structural complexity collectively represent useful indicators of hydrothermal activity. Similar relationships have been documented in other volcanic geothermal systems where alteration, fracturing, and fluid circulation modify the physical properties of the host rocks (e.g., Okubo et al., 1985; Arnason, 1995; Pandarinath et al., 2019).

The overall architecture of the proposed hydrothermal system shows notable similarities to the conceptual model for the San Pedro Domes geothermal field (Reyes-Orozco et al., 2019), in which hydrothermal alteration, elevated temperatures, and basement–controlled fluid circulation have also been documented. In both cases, the volcanic sequence overlies basement rocks of the Jalisco Block, and geothermal activity appears to be strongly influenced by fault–controlled permeability and lithological contrasts. This correspondence suggests that both systems may share common tectonic and thermal controls within the San Pedro–Ceboruco Graben and may form part of a broader geothermal province associated with regional extensional tectonics and late Quaternary volcanism.

Although additional drilling, petrophysical characterization, and subsurface imaging are required to validate the proposed system geometry, the integrated geophysical and geothermal evidence supports the presence of a structurally controlled volcanic–hydrothermal system characterized by elevated heat flow, shallow thermal anomalies, pervasive faulting, and extensive hydrothermal alteration. Together, these characteristics provide a coherent framework for evaluating the geothermal significance of the Amado Nervo volcanic complex and establish the basis for the geothermal potential assessment presented in the following section.

5.3. Geothermal implications, uncertainties, and limitations

The estimated geothermal potential of the Amado Nervo volcanic system should be interpreted in the context of both supporting geophysical evidence and the uncertainties associated with the adopted resource–assessment methodology. The proposed reservoir geometry is based on integrating gravity anomalies, magnetic attenuation, analytical signal patterns, geothermal–gradient estimates, and the conceptual hydrothermal model developed in this study. Collectively, these observations suggest a structurally controlled hydrothermal system characterized by enhanced fracturing, hydrothermal alteration, and elevated thermal gradients. The inferred reservoir beneath the volcanic sequence and within the fractured crystalline basement is therefore consistent with the available geophysical constraints, although its geometry and continuity remain unverified by deep drilling.

The comparison with the San Pedro Domes geothermal field provides additional evidence supporting the plausibility of the proposed model. Similarities in structural setting, estimated reservoir temperatures, depth to basement, and evidence of hydrothermal alteration may indicate that both systems share common tectonic and thermal controls within the San Pedro–Ceboruco Graben. Nevertheless, these similarities should not be interpreted as proof of equivalent reservoir properties, as significant differences in permeability, fluid chemistry, reservoir volume, and thermal recharge may exist between the two systems.

The Heat in Place assessment provides a first–order estimate of the geothermal resource and suggests that the Amado Nervo volcanic system may possess a resource capable of supporting small– to medium–scale geothermal development. However, the uncertainty associated with the estimate remains substantial, as reflected by the wide range of simulated outcomes. This uncertainty arises from the limited availability of direct subsurface information and from the assumptions required to define key model parameters. Several of these parameters were adopted from published geothermal studies, theoretical ranges reported in the literature, or analogies with nearby geothermal systems such as San Pedro Domes. Consequently, the resulting geothermal potential should be regarded as a preliminary estimate rather than a proven resource.

Additional uncertainty stems from assumptions regarding reservoir thickness, areal extent, porosity, recovery factor, thermal properties, and reservoir temperature distribution. Moreover, the Curie–point–depth–derived geothermal gradient represents an average crustal thermal condition and may not fully capture local thermal heterogeneity associated with fault–controlled fluid circulation. Likewise, the conceptual reservoir geometry remains dependent on indirect geophysical evidence and has not yet been validated through exploratory drilling or detailed reservoir characterization.

Despite these limitations, the convergence of multiple independent datasets–including gravity anomalies, magnetic anomalies, analytical signal attenuation, Curie point depth estimates, geothermal gradients, and regional geological and hydrogeological information–provides a coherent framework supporting the geothermal prospectivity of the Amado Nervo volcanic system. The estimated resource magnitude places the system within the range reported for several medium–scale geothermal projects in Mexico, including San Pedro Domes (35.5 mW), Las Tres Vírgenes (10 MW), and Cerritos Colorados (5–15 MW). Although substantially smaller than major geothermal fields such as Cerro Prieto (500 MW) or Los Azufres (240 MW), the resource estimate suggests that Amado Nervo may represent a viable target for future geothermal exploration. Further progress will require exploratory drilling, detailed geochemical studies, reservoir modeling, and economic evaluation to reduce uncertainty and determine the technical feasibility of geothermal development.

6. Conclusions

This study integrated geological information, gravity and magnetic data, geothermal gradient measurements, and spectral magnetic analysis to develop a conceptual hydrothermal model for the Amado Nervo volcanic system. The combined geophysical evidence reveals a structurally controlled volcanic framework characterized by significant density and magnetization contrasts, suggesting fractured and hydrothermally altered domains associated with the regional fault network.

Gravity and magnetic anomalies delineate zones of reduced density and attenuated magnetization beneath the Amado Nervo Volcano, Cerro Las Tetillas, and the San Pedro Domes area. These geophysical signatures are spatially associated with major regional structures, including the Milpillas–Cerro Grande, Borbollón, and Las Cebollas fault systems, highlighting the importance of tectonic controls on volcanic evolution, structural permeability, and hydrothermal fluid circulation.

Spectral analysis of the reduced-to-the-pole magnetic anomaly yielded a Curie point depth of approximately 7.5 km, from which a geothermal gradient of ~70.8 $°C \cdot km^{-1}$ and a conductive heat flow of ~176 $mW \cdot m^{-2}$ were estimated. These values are consistent with previously reported geothermal gradients in the region and support the existence of an elevated thermal regime beneath the Amado Nervo volcanic complex. The resulting conceptual model is compatible with a vertically organized volcanic–hydrothermal system in which a residual intrusive heat source may sustain hydrothermal activity at depth.

Integration of available geophysical, geological, and geothermal information suggests the presence of a potential geothermal reservoir beneath the inferred cap sequence rock and within the fractured crystalline basement rocks. Estimated temperatures of approximately 150 °C at depths of 1.5–1.7 km indicate conditions that may be favorable for geothermal development and provide a preliminary target for future exploration drilling.

Application of the volumetric Heat in Place method coupled with 9,999 Monte Carlo simulations yielded a preliminary geothermal potential estimate of 19.75 ± 14.41 MW, with simulated values ranging from approximately 5 to 34 MW. Although this estimate is subject to uncertainty associated with reservoir geometry, thermal parameters, recovery factors, and the limited availability of direct subsurface information, it places the Amado Nervo volcanic system within the range of medium–scale geothermal prospects reported in Mexico.

Overall, the results support the geothermal prospectivity of the Amado Nervo volcanic complex and justify continued exploration efforts, including exploratory drilling, detailed geochemical investigations, hydrogeological characterization, and reservoir modeling. While the proposed conceptual model remains constrained primarily by indirect geophysical evidence, the integrated methodology applied here provides a robust framework for geothermal assessment. It may be transferable to other volcanic regions of the Jalisco Block and the Trans–Mexican Volcanic Belt.

7. References

Arnason, S. 1995. Geothermal systems in Iceland: Structure and conceptual models–I. High–temperature areas. Geothermics, 24 (5–6), 561–602 pp. https://doi.org/10.1016/0375-6505(95)00025-9

Blakely, R.J. 1996b. Regional gravity fields. In: Potential theory in gravity and magnetic applications. Cambridge University Press. United Kingdom. 128–153 pp. https://doi.org/10.1017/CBO9780511549816

CENAPRED, Centro Nacional de Prevención de Desastres. 2019. Sistema de información sobre riesgos. Available at: http://www.atlasnacionalderiesgos.gob.mx/archivo/visor-capas.html. Accessed: July 2025.

CONAGUA, Comisión Nacional del Agua. 2025. Sistema Nacional de Información del Agua. Available at: https://sina.conagua.gob.mx/. Accessed: July 2025.

Espinoza–Ojeda, O. M., Prol–Ledesma, R. M., Muñiz–Jauregui, J. A. 2023. Update and Review of Continental Conductive Surface Heat Flow Measurements in México: An Analysis of Deep Boreholes. Natural Resources Research, 32. https://doi.org/10.1007/s11053-023-10173-9.

Fedi, M., Quarta, T., De Santis, A. 1997. Inherent power–law behavior of magnetic field power spectra from a Spector and Grant ensemble. Geophysics: 62 (4), 1143–1150 pp. https://doi.org/10.1190/1.1444215

Fernández–Córdoba, J., Zamora–Camacho, A., Espíndola, J.M. 2017. Gravity Survey at the Ceboruco Volcano area (Nayarit, Mexico): a 3–D model of the subsurface structure. Pure and Applied Geophysics: 174 (10), 3905–3918 pp. https://doi.org/10.1007/s00024-017-1600-4.

Ferrari, L., Pasquere, G., Venegas–Salgado, S., Romero–Ríos, F. 1999. Geology of the western Mexican Volcanic Belt and adjacent Sierra Madre Occidental and Jalisco Block. In: Delgado–Granados, H., Aguirre–Díaz, G.J., Stock, J.M. (Eds.), Cenozoic Tectonics and Volcanism of Mexico. Geological Society of America, Boulder, Colorado https://doi.org/10.1130/SPE334 Special Paper: 334 pp

Ferrari, L., Petrone, C.M., Francalanci, L., Tagami, T., Eguchi, M., Conticelli, S., Manetti, P., Venegas–Salgado, S., 2003. Geology of the San Pedro–Ceboruco Graben western Trans–Mexican Volcanic Belt. Revista Mexicana de Ciencias Geológicas, 20 (3), 165–181. Available at: https://rmcg.geociencias.unam.mx/index.php/rmcg/article/view/918/765 Accessed: July 2025.

Ferrari, L., Orozco-Esquivel, T., Manea, V., Manea, M., 2012. The dynamic history of the Trans–Mexican Volcanic Belt and the Mexico subduction zone. Tectonophysics, 522–523 (2012), 122–149. https://doi.org/10.1016/j.tecto.2011.09.018

Fuentes–Arreazola, M. A., Núñez, D., Núñez–Cornú, F.J., Calderón–Moctezuma, A., Ruiz–Aguilar, D., Romo–Jones, J.M. 2021. Magnetotelluric imaging of the Ceboruco

Volcano, Nayarit, Mexico. Journal of Volcanology and Geothermal Research: 418, 12 pp. https://doi.org/10.1016/j.jvolgeores.2021.107339.

Fuentes–Arreazola, M. A., Núñez, D., Cupul–Velázquez, A.M., Núñez–Cornú, F.J. 2023. New insights into El Chichón (Chiapas, Mexico) hydrothermal system from an aeromagnetic survey. Journal of South American Earth Sciences: 122. https://doi.org/10.1016/j.jsames.2022.104169

Garg, S.K., Combs, J. 2015. A reformulation of the USGS volumetric “Heat in Place” resource estimation method. Geothermics: 55, 150–158 pp. https://doi.org/10.1016/j.geothermics.2015.02.004

Hanley, R.W., Ellis, A.J. 1983. Geothermal systems, ancient and modern: a geochemical review. Earth–Science Reviews, 19 (1): 1–50 pp. https://doi.org/10.1016/0012-8252(83)90075-2

Hildenbrand, T.G., Briesacher, A., Flanagan, G., Hinze, W.J., Hittelman, A.M., Keller, G.R., Kucks, R.P., Plouff, D., Roest, W., Seeley, J., Smith, D.A., Webring, M. 2002. Rationale and operational plan to upgrade the U.S. Gravity Database. In: U.S. Geological Survey OpenFile Report 02-463, pp. 12. Available at: https://pubs.usgs.gov/publication/ofr02463 Accessed: July 2025.

Hiriart–Le Bert, G., Gutiérrez–Negrín, L.C.A., Quijano–León, J.L., Ornelas–Celis, A., Espíndola, S., Hernández, I. 2011. Evaluación de la Energía Geotérmica en México, Informe para el Banco Interamericano de Desarrollo y la Comisión Reguladora de Energía, Ciudad de México, México.167 pp. Available at: http://www.cre.gob.mx/documento/2026.pdf Accessed: July 2025.

Hirt, C., Claessens, S.J., Fecher, T., Kuhn, M., Pail, R., Rexer, M. 2013. New ultrahigh–resolution picture of the Earth’s gravity field. Geophysical Research Letters: 40 (16) 4279–4283 pp. https://doi.org/10.1002/grl.50838

IGRF, International Geomagnetic Reference Field. 1980. In: International Association of Geomagnetism and Aeronomy. Division V–Mod, Geomagnetic Field Modeling. Available at: http://www.ngdc.noaa.gov/IAGA/vmod/igrf_old_models.html. Accessed: July 2025.

INEGI, Instituto Nacional de Estadística y Geografía. 2025. Mapa Digital de México. Available at: http://gaia.inegi.org.mx/mdm6/. Accessed: July 2025.

Muffler, P., Cataldi, R. Methods for regional assessment of geothermal resources. Geothermics: 7 (2–4) 53–89 pp. https://doi.org/10.1016/0375-6505(78)90002-0

Muñoz–Burbano, F., Calo, M., Savard, G., Reyes–Orozco, V., Lupi, M. 2024. Using time–lapse seismic velocity changes to monitor the Domo San Pedro geothermal field, Mexico. Geothermics: 120: 13 pp. https://doi.org/10.1016/j.geothermics.2024.103010

Nelson, S.A. 1980. Geology and petrology of Volcan Ceboruco, Nayarit, Mexico. Geological Society of American Bulletin, 91. https://doi.org/10.1130/GSAB-P2- 91-2290

Núñez–Cornú, F.J., Escalona–Alcázar, F.J., Núñez–Escribano, D., Trejo–Gómez, E., Suárez–Plascencia, C., Rodríguez–Ayala, N. 2020. Study of seismic activity at

Ceboruco Volcano (Nayarit, Mexico) in the period 2012 to 2014. Journal of South American Earth Sciences: 98. https://doi.org/10.1016/j.jsames.2019.102473.

Núnez–Demarco, P., Prezzi, C., Sánchez–Bettucci, L. 2020. Review of Curie point depth determination through different spectral methods applied to magnetic data. Geophysical Journal International: 224 (1), 17–39 pp. https://doi.org/10.1093/gji/ggaa361

Núñez, D., Núñez–Cornú, F.J., Rowe, C.A. 2022. Recent Seismicity at Ceboruco Volcano (Mexico). Journal of Volcanology and Geothermal. Research: 421. https://doi.org/10.1016/j.jvolgeores.2021.107451

Okubo, Y., Graf, R.J., Hansen, R.O., Ogawa, K., Tsu, H. 1985. Curie point depth of the island of Kyushu and surrounding areas, Japan. Geophysics: 50 (3), 481–494 pp. https://doi.org/10.1190/1.1441926

Pandarinath, K., Shankar, R., Santoyo, E., Shetty, S.B., García–Soto, A.Y., González–Partida, E. 2019. A rock fingerprint of hydrothermal alteration in volcanic rocks: An example from the Los Azufres geothermal field, Mexico. Journal of South American Earth Sciences: 91, 260–271. https://doi.org/10.1016/j.jsames.2019.02.018

Petrone, C.M., Tagami, T., Francalanci, L., Matsumara, A., Sudo, M., 2001. Volcanic systems in the San Pedro–Ceboruco graben (Nayarit, Mexico) in the light of new K–Ar geochronological data. Geochemical Journal, 35 (2), 77–88. https://doi.org/10.2343/geochemj.35.77

Prol–Ledezma, R.M., Morán–Zenteno, D.J. 2019. Heat flow and geothermal provinces in Mexico. Geothermics (78): 183–200 pp. https://doi.org/10.1016/j.geothermics.2018.12.009

Ravat, D., Pignatelli, A., Nicolisi, I., Chiappini, M. 2007. A study of spectral methods of estimating the depth to the bottom of magnetic sources from near-surface magnetic anomaly data. Geophysical Journal International: 169 (2), 421–434 pp. https://doi.org/10.1111/j.1365-246X.2007.03305.x

Reyes–Orozco, V.M., Avalos–Tapia, D., García–Tirado, J., Rodríguez–Pineda, E., Ocampo–Aguilar, F. 2019. Preliminary conceptual model of the Domo San Pedro geothermal field, western sector of Trans–Mexican Volcanic Belt, Nayarit, Mexico. Proceedings of the 44th Workshop on Geothermal Reservoir Engineering, Stanford, California, February 11–13, 2019. Available at: https://pangea.stanford.edu/ERE/pdf/IGAstandard/SGW/2019/Reyes.pdf Accessed: July 2025.

Rodríguez, E., Ocampo, F., Reyes–Orozco, V., Ávalos, D., García, J. 2019. Preliminary geochemica model of the Domo San Pedro geothermal field in San Pedro Lagunillas, Mexico. Proceedings of the 44th Workshop on Geothermal Reservoir Engineering, Stanford, California, February 11–13, 2019. Available at: https://pangea.stanford.edu/ERE/pdf/IGAstandard/SGW/2019/Rodriguez.pdf Accessed: July 2025.

Rodríguez–Uribe, M.A., Núñez–Cornú, F.J., Nava–Pichardo, F.A., Suárez–Plascencia, C. 2013. Some insights about the activity of the Ceboruco Volcano (Nayarit, Mexico) from recent seismic low-frequency activity. Bulletin of Volcanology: 75, 755 pp. https://doi.org/10.1007/s00445-013-0755-9.

Sánchez, J.J., Núñez–Cornú, F.J., Suárez–Plascencia, C., Trejo–Gómez, E. 2009. Seismicity at Ceboruco Volcano, Mexico. Seismology Research Letters: 80 (5), 823–830 pp. https://doi.org/10.1785/gssrl.80.5.823

Sawires, R., Aboud, E. 2019. Subsurface structural imaging of Ceboruco Volcano area, Nayarit, Mexico, using high–resolution aeromagnetic data. Journal of. Volcanology and Geothermal Research: 371, 162–176 pp. https://doi.org/10.1016/j.jvolgeores.2019.01.012

SGM, Servicio Geológico Mexicano. 2005. Carta magnética de campo total, escala 1: 50,000, Compostela F13–D41. Available at: https://mapserver.sgm.gob.mx/Cartas_Online/geofisica/907_F13-D41_GF.pdf Accessed: July 2025.

Seequent Ltd. 2025. Oasis montaj ® Geoscience Plataform. Seequent Ltd. Christchurch, New Zealand.

Servicio Geológico Mexicano, SGM, 2025. GEOINFOMEX. Available at: https://www.sgm.gob.mx/GeoInfoMexGobMx/ Accessed: July 2025.

Seigel, H.O. 1995. A guide to high precision land gravimetric surveys. Scintrex. Ontario, Canada. 132 pp. Available at: https://scintrexltd.com/wp-content/uploads/2017/02/Guide-High-Precision-Land-Gravimeter-Surveys.pdf Accessed: July 2025.

Sieron, K., Siebe, C. 2008. Revised stratigraphy and eruption rates of Ceboruco stratovolcano and surrounding monogenetic vents (Nayarit, Mexico) from historical documents and new radiocarbon dates. Journal of Volcanology and Geothermal Research: 176 (2), 241–264 pp. https://doi.org/10.1016/j.jvolgeores.2008.04.006.

Stock, J.M. 1993. Tectónica de placas y evolución del Bloque Jalisco, México. GEOS Boletín de la Unión Geofísica Mexicana: 13 (3), 3–9 pp. Available at: https://geos.cicese.mx/index.php/geos/article/view/314 Accessed: July 2025.

Tanaka, A., Okubo, Y., Matsubayashi, O. 1999. Curie point depth based on spectrum analysis of the magnetic anomaly data in East and Southeast Asia. Tectonophysics: 306 (3–4), 461–470 pp. https://doi.org/10.1016/S0040-1951(99)00072-4.

Telford, W.M., Geldart, L.P., Sheriff, R.E., Keys, D. 1990. Magnetic methods. In: Applied geophysics. Second edition. Cambridge University Press., New York, EE. UU. 62–135 pp. https://doi.org/10.1017/CBO9781139167932

Tello-Hinojosa, E., 1994. Geochemistry of the thermal springs around the Ceboruco Volcano, Nayarit, Mexico. Geotermia Rev. Mexicana Geoenergia 10 (2), 3–8.

Turcotte, D.L., Schubert, G., 2002. Heat transfer. In: Geodynamics. Cambridge University Press, Cambridge. 132–194 pp. https://doi.org/10.1017/CBO9780511807442.006

Venegas, S. 1995. Geothermal exploration results at the Ceboruco Volcano, Nayarit State, Mexico. Geotermia, Revista Mexicana de Geoenergía: 11 (2), 71–86 pp.

8. Acknowledgements

We sincerely thank the Editor and Reviewers for their careful evaluation of the manuscript and for their constructive comments and suggestions. Their observations significantly improved the study's clarity, organization, scientific rigor, and overall readability. The authors gratefully acknowledge the Programa Interinstitucional para el Fortalecimiento de la Investigación y el Posgrado del Pacífico (Programa Delfín) for supporting the 2023 undergraduate research stay, during which the initial geophysical analyses that contributed to the development of this study were undertaken. This work represents the subsequent scientific development and integration of those initial research efforts into the conceptual hydrothermal model and geothermal assessment presented herein.